10.64837/GSA.13.5.2

Global and Stochastic Analysis

Vol. 13 No. 5 (2026)

Received: 18th June 2026 Revised: 15th August 2026 Accepted: 06th September 2026

STOCHASTIC FRACTIONAL MODELING OF HIV-TB CO-INFECTION WITH ENVIRONMENTAL TRANSMISSION EFFECTS

G. KARUPPANNAN AND A. MANICKAM*

Abstract. In order to better anticipate disease transmission patterns, this research suggests a Caputo type fractional-order differential equations model for HIV-TB co-infection that accounts for reserves in the environment of Mycobacterium tuberculosis and memory effects. The existence, uniqueness, positivity, boundedness, and Ulam-Hyers stability studies demonstrate that the model is mathematically well-posed. The Adams-Bashforth-Moulton predictor-corrector approach is used to build numerical solutions, which are calibrated using HIV-TB data from Tanzania between 2000 - 2023. Significant memory effects associated with treatment persistence, environmental contamination, and infection history are demonstrated by the expected fractional order ($\omega = 0.982$).The model's robustness and applicability are demonstrated through validation using Kenyan data. Sensitivity analysis identifies the crucial factors that affect the spread and management of disease. The fractional-order formulation more accurately captures long-term infection trends and fits the real data better than the conventional integer-order model. According to the study, HIV-TB co-infection can be considerably decreased and disease management in high-burden settings improved by combining medical therapy with environmental control measures.

Keywords: Caputo Fractional Differential Equation; HIV; Tuberculosis; Stability Analysis;

Mathematical Subject Classification: 26A33,34C60,65D05

1. Introduction

Tuberculosis (TB) and the Human Immunodeficiency Virus (HIV) continue to constitute a serious threat to world health, with their combined effects being most noticeable in sub-Saharan Africa [1]. By gradually reducing CD4+ T cells, HIV compromises host defense and increases susceptibility to a variety of opportunistic diseases, of which tuberculosis (TB) is still the most common and lethal, especially in environments with limited access to early diagnosis and long-term treatment [2]. Co-infection is still a major source of morbidity and mortality in many low- and middle-income countries, despite significant advancements in TB treatment and antiretroviral medication While TB infection boosts HIV viral replication and accelerates the onset of acquired immunodeficiency syndrome (AIDS), HIV weakens the immune system, making a person more vulnerable to TB infection and reactivation. HIV and TB have a mutually reinforcing relationship that greatly speeds up the course of the disease, raises mortality, and makes treatment more difficult. The efficacy of single-disease therapies is compromised by these feedback processes, which further complicate therapeutic management. Because of this, co-infection between HIV and TB presents special difficulties that cannot be sufficiently resolved

Corresponding author: A. Manickam (Email address: manickammaths2011@gmail.com)

by treating each illness separately. For co-infected persons, integrated treatment approaches are required due to the different clinical courses and therapeutic approaches for HIV and TB. Given its effective and limited regimen, standard practice requires that TB treatment be started as soon as possible. However, there is a therapeutic conundrum regarding the timing of ART commencement. Immune Reconstitution Inflammatory Syndrome (IRIS), a disorder marked by worsening TB symptoms and serious consequences that may result in treatment stoppage, may be triggered by starting ART concurrently with or soon after TB treatment. Conversely, postponing antiretroviral therapy until the completion of tuberculosis treatment elevates the risk of HIV-related mortality and future transmission. Consequently, one of the most important unmet needs in co-infection care is figuring out the best combination therapy protocol. Caputo type fractional-order differential equations model, which better represent biological processes including memory effects and complex nonlinear interactions, are gaining popularity in disease modeling. Artificial intelligence and neural networks frequently improve these methods, increasing analysis, numerical approximation, and prediction accuracy. These hybrid frameworks can be used to solve complex fractional integro-differential equations, analyse epidemic models, predict viral eye infections, model chronic myeloid leukemia, and even model psychiatric disorders. These hybrid approaches reinforce the applicability of the current fractional HIV-TB paradigm by highlighting the increasing significance of fusing sophisticated computational methods with mechanistic fractional-order models. Motivated by these advancements, this study employs a fractional-order modeling framework to more precisely represent the dynamics of HIV and TB co-infection transmission. Understanding HIV-TB transmission and assessing therapeutic tactics have long relied on mathematical models [3]. Classical integer-order models provide valuable insights into disease dynamics and control strategies, even though they may overlook long-term memory effects, host variability, and delays associated with treatment adherence or environmental persistence. In order to get around these limitations, fractional-order models particularly those based on the Caputo derivative have become more and more prominent in epidemiological research. These models inherently include nonlocal dynamics and memory effects, which are particularly pertinent to long-term conditions like HIV and TB. The Caputo derivative is ideal for realistic epidemiological modeling because it permits physically significant initial conditions. Recent studies have applied Caputo fractional-order frameworks to HIV-only, TB-only, and HIV-TB co-infection models. Compared to their integer-order counterparts, fractional-order operators exhibit improved stability features, better agreement with epidemiological data, and improved model accuracy by incorporating nonlocal temporal effects. For example, and shown how fractional derivatives have a substantial impact on system dynamics, exposing disease-control mechanisms that traditional models could miss. Subsequent research has demonstrated that integrated techniques can almost completely eradicate infections assuming adequate compliance, highlighting the usefulness of fractional-order differential equations in optimum control design [4]. Demonstrated the benefits of fractional modeling in co-infection management by highlighting the combined impact of HIV prevention and TB therapy. However, Most existing models either oversimplify environmental transmission or overlook the significance of environmental TB reservoirs, Notwithstanding data showing that, especially in high-burden environments, polluted environments have a major role in TB persistence. Therefore, a true representation of TB dynamics must include environment-mediated TB

transmission. Interventions that solely target human populations may be undermined by environmental reservoirs acting as chronic sources of infection. Explicitly modeling environmental TB contamination offers a more comprehensive framework for assessing the combined effects of medical treatments and environmental control measures, such as hygiene and sanitation, on disease dynamics. There are still a number of significant gaps in the large set of mathematical models created to investigate HIV-TB co-infection. The majority of current models either only contain human-to-human transmission pathways and ignore the significance of environmentally produced TB persistence, or They rely on conventional integer-order formulations that disregard the memory effects that come with long-term infections. Moreover, very few research examine the combined effects of environmental and medical interventions within an ideal control framework, and even fewer incorporate actual epidemiological data to calibrate fractional-order co-infection models. In contrast to current HIV-TB models, this study simultaneously takes into account environmental TB reservoirs, fractional memory effects using the Caputo derivative, data-driven parameter estimation using Tanzanian HIV-TB co-infection data reported by the WHO, and the best way to implement environmental and medical control measures within a single modeling framework [5]. This comprehensive approach not only yields a more accurate representation of HIV-TB transmission dynamics but also offers valuable insights for the development of integrated, data-driven, and sustainable disease management strategies in high-burden settings. The structure of the paper is as follows: The model and its underlying presumptions are presented in Section 2. The qualitative aspects of the model, such as parameter estimations, sensitivity analysis, Ulam-Hyers stability, and the PECE-ABM technique, are examined in Section 3. Section 4 addresses the optimal control formulation, effective reproduction number, and prerequisites for optimality in the context of the HIV-TB co-infection model with control measures. Numerical simulations and control results are presented and discussed in Section 5. The key conclusions and their policy implications are presented in Section 6.

2. Model Construction and Formulation

In order to represent memory-dependent disease dynamics, a fractional differential order HIV-TB co-infection model was developed utilizing the Caputo type derivative. For chronic illnesses like HIV and TB, where current transmission patterns are influenced by rapid exposure, delayed immune responses, treatment compliance, and environmental persistence, fractional calculus is particularly helpful. A number of modelling assumptions are used in order to concentrate on the key mechanisms controlling HIV-TB co-infection. The vulnerable population is expected to be recruited at a constant rate ρ. It is assumed that the population is homogeneous. It is believed that susceptible people cannot become co-infected since they cannot contract both HIV and TB at the same time. The model makes the assumption that HIV does not spread vertically, from mother to kid [6]. It is believed that both direct contact with infected people and exposure to contaminated environments can spread tuberculosis. People who have both active TB and HIV are thought to be extremely immunocompromised. Sexual activity within this class is deemed insignificant due to their clinical status; hence, sexual transmission of HIV from this compartment is disregarded. ART recipients are presumed to be aware of their HIV status, to be undergoing treatment, and to participate in activities that prevent the virus from spreading. According to WHO standards, Screening for TB is presumed to take place at both

during the follow-up period and at the time of HIV diagnosis, with co-infected persons receiving TB treatment right away. As a result, the model presupposes that among co-infected patients, TB therapy comes before HIV treatment. TB treatment is typically administered for six to nine months. Additionally, it is believed that those under treatment for TB or HIV make very little contribution to subsequent transmission. It is assumed that people on antiretroviral therapy (ART) are aware of their HIV status, are receiving treatment, and engage in behaviors that stop the virus from spreading. TB screening is assumed to occur at the time of HIV diagnosis and during the follow-up period, with co-infected individuals receiving immediate TB treatment, according to World Health Organization guidelines. Transmission from treated individuals is thus disregarded because the model focuses on the population level. Due to persistent viral suppression, those who recover from tuberculosis while still receiving antiretroviral therapy are regarded as non-infectious. Finally, co-infected individuals are thought to adopt habits that reduce their chance of re-infection if they maintain antiretroviral therapy after recovering from tuberculosis. These presumptions lead to the stratification of the entire human population $P(t)$ into nine disjoint incompatible compartments: Susceptible (S), Latent tuberculosis $[L_t(t)]$, Active tuberculosis $[A_T(t)]$, Recovered from tuberculosis $[R_T(t)]$, HIV-positive $[H_I(t)]$, Regarding ART $[A_H(t)]$, Latent TB and HIV co-infection $[M_1(t]$, HIV-active TB co-infected $[M_2(t]$, and co-infected while receiving TB treatment $[C_T(t]$. The concentration of ambient TB bacilli is modeled in a tenth compartment. Consequently:

$$P(t) = S(t) + [L_t(t)] + [A_T(t)] + [R_T(t)] + [H_I(t)] + [A_H(t)] + [M_1(t] + [M_2(t] + [C_T(t] \quad (2.1)$$

Direct and environmental channels are included in the force of infection for tuberculosis, orF_T:

$$F_T = \left[\frac{\alpha_T}{P}(A_T + \mu_1 M_2) + \alpha_1 E_b\right] \quad (2.2)$$

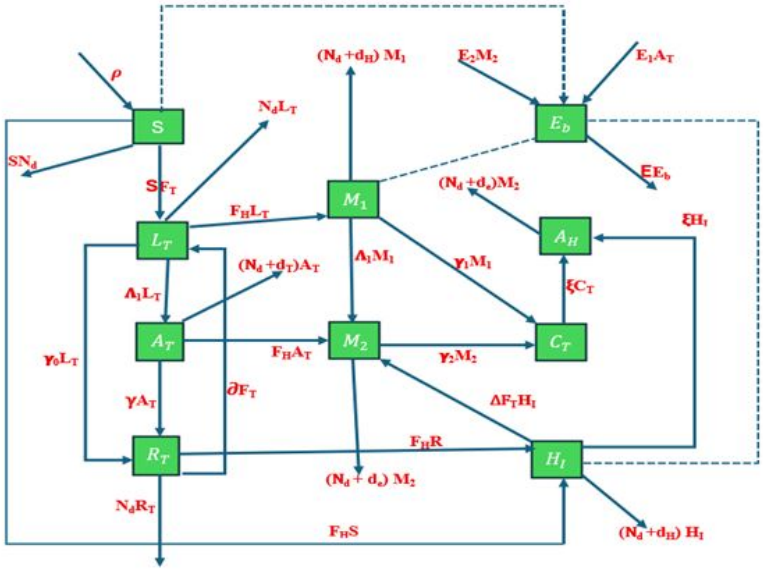
where $\mu_1 > 1$ increases the infectiousness of M_2 individuals, α_T is the rate of direct tuberculosis transmission , and α_1 is the ambient infection rate. Contact with infectious compartments is taken into account by the HIV force of infection, or F_H

$$F_H = \frac{\alpha_H}{P}(H_I + \mu_2 M_1) \quad (2.3)$$

where μ_2 is an individual's increased infectivity and α_H is the HIV transmission rate. The rates at which susceptible people can contract HIV or TB are F_T and F_H respectively. Individuals in the latent TB class $[L_T]$ may either develop HIV at rate $[F_H]$ or advance to active TB at rate Λ_1. Additionally, individuals in the Latent class can transition to the recovery group after beginning TB therapy at a rate of γ_0. People with active TB $[A_T]$ may also get HIV at rate $[F_H]$, begin TB treatment at rate γ, and pass away from TB-related problems at rate d_T. Recovered persons R_T may be partially re-infected with TB at rate ∂F_T, where $\partial \in [0, 1]$ represents the degree of immunity from prior TB infection. They are also vulnerable to HIV infection at a rate F_H Due to immunosuppression ($\Delta > 1$), HIV-positive individuals H_I may develop TB at a higher rate $\Delta\Lambda_1$ start ART at a rate ξ, or pass away from HIV-related illnesses at a rate d_H. People in class $[M_1]$ may develop active TB co-infection $[M_2]$ at a rate Λ_2, die at a rate Λ_2, or start TB treatment at a rate that is in line with recommendations that prioritize TB treatment over ART. The environmental bacterial load $[E_b]$ increases through shedding from $[A_T]$ and $[M_2]$ (rates $[K_1]$, $[K_2]$) decays naturally at rate $[E]$. Individuals in $[C]$ may then start ART and move to at rate ξor die from disease-related causes at rate $[d_e]$. Natural mortality

occurs in every human compartment at a rate $[N_d]$. Fig. 1 summarizes the outcomes of the aforementioned.

FIGURE 1. System diagram



2.1. Caputo Fractional Differential Equation Model. The substantial memory and genetic effects seen in HIV-TB co-infection dynamics provide biological motivation for the fractional order formulation used in this investigation. While tuberculosis shows protracted latency, partial immunity, and reactivation after prolonged periods, HIV progression is defined by cumulative immune system deterioration, delayed virological response to antiretroviral therapy, and long-term treatment history [7]. Further temporal reliance is introduced by the persistence of Mycobacterium tuberculosis in contaminated environments, since the risk of infection is dependent on past pathogen shedding and environmental contamination levels in addition to current conditions. Therefore these effects are represented by the Caputo fractional derivative, which preserves biologically significant initial circumstances while allowing the current rate of change to depend on the system's whole history. Mathematically speaking, This demonstrates how each state variable varies according to an integral of the convolution type over its prior values. The Caputo fractional derivative, which is explained below, formalizes this. Because of this, the fractional-order derivative provides a realistic representation of treatment adherence history, environmental persistence, and delayed immune responses that are not adequately captured by conventional integer order models. To achieve dimensional consistency in the fractional order HIV-TB co-infection model, we use a fractional time scaling method that is commonly used

with Caputo derivatives. Given that the dimension of the Caputo derivative of order $\omega \in (0,1]$ is dimension $[time]^{-\omega}$.

classical rate parameters must be rescaled in order to preserve dimensional homogeneity of the governing equations. As a result, the model's mathematical coherence is restored by raising all time-dependent parameters to the fractional order ω. This scaling is a mathematical technique that enables integer order parameters to be consistently incorporated inside a fractional order framework, rather than a true biological adjustment of epidemiological rates [8]. A well-established method in fractional epidemiological modeling, the fractional order ω biologically represents memory effects related to treatment history, environmental persistence, and chronic infection [9,10].

$$F_T^C = \left[\frac{\alpha_T^\omega}{P}(A_T + \mu_1 M_2) + \alpha_1^\omega E_b\right] \ \ and \ \ F_H^C = \frac{\alpha_H^\omega}{P}(H_I + \mu_2 M_1) \tag{2.4}$$

The following system of nonlinear fractional differential equations under the Caputo type fractional derivative describes the dynamics of HIV-TB co-infection, taking into account the model flow diagram [Figure 1]

system of equations

$$\begin{aligned}
{}_0^cD_t^\omega S(t) &= \rho^\omega - (F_T^c + F_H^c + N_d^\omega)S \\
{}_0^cD_t^\omega L_T(t) &= F_T^c S + \partial F_T^c R_T - (N_d^\omega + \Lambda_1^\omega + \gamma_0^\omega + F_H^c)L_T \\
{}_0^cD_t^\omega A_T(t) &= \Lambda_1^\omega L_T - (N_d^\omega + d_T^\omega + \gamma^\omega + F_H^c)A_T \\
{}_0^cD_t^\omega R_T(t) &= \gamma^\omega A_T + \gamma_0^\omega L_T - (N_d^\omega + \partial F_T^c + F_H^c)R_T \\
{}_0^cD_t^\omega E_b(t) &= E_1^\omega A_T + E_2^\omega M_2 - E^\omega E_b \\
{}_0^cD_t^\omega H_I(t) &= F_H^c S + F_H^c R_T - (N_d^\omega + d_H^\omega + \Delta F_T^c + \xi^\omega)H_I \\
{}_0^cD_t^\omega A_H(t) &= \xi^\omega H_I + \xi^\omega C_T - (N_d^\omega + d_H^\omega)A_H \\
{}_0^cD_t^\omega M_1(t) &= F_H^c L_T - (N_d^\omega + \Lambda_2^\omega + d_H^\omega + \gamma_1^\omega)M_1 \\
{}_0^cD_t^\omega M_2(t) &= \Lambda_2^\omega M_1 + \Delta F_T^c H_I + F_H^c A_T - (N_d^\omega + d_e^\omega + \gamma_2^\omega)M_2 \\
{}_0^cD_t^\omega C_T(t) &= \gamma_1^\omega M_1 + \gamma_2^\omega M_2 - (N_d^\omega + \xi^\omega + d_e^\omega)C_T \\
S(0) &> 0, L_T(0) \geq 0, A_T(0) \geq 0, R_T(0) \geq 0, \\
E_b(0) \geq 0, H_I(0) &\geq 0, A_H(0) \geq 0, M_1(0) \geq 0, M_2(0) \geq 0, C_T(0) \geq 0.
\end{aligned} \tag{2.5}$$

3. Qualitative Analysis of the HIV-TB Co-Infection Model

We examine the qualitative properties of the proposed fractional-order differential equations HIV-TB co-infection model and local stability of the disease-free equilibrium, Ulam-Hyers stability, well-posedness, and computation of the basic reproduction number. The appendices contain comprehensive technical proofs.

Theorem 3.1. *Equations (2.5) has a unique solution that is non-negative for every $t \geq 0$. for any non-negative initial conditions.*

TABLE 1

Parameters	Discription
ρ	Birth rate of susceptible people or recruitment rate
α_H	HIV transmission rate
α_T	TB transmission coefficient
N_d	Death rate of natural
d_T	TB related death rate
d_H	HIV related death rate
d_e	Co infection related death rate
α_1	Coefficient of environmental tuberculosis transmission
ξ	Rate of HIV therapy
μ_1	TB transmission amplification factor in co-infected people $[M_2]$
μ_2	TB transmission amplification factor in co-infected people $[M_1]$
Δ	HIV-positive people's TB progression multiplier
∂	Modifier of re-infection risk
Λ_1	The rate at which latent tuberculosis develops into active tuberculosis in people without HIV
Λ_2	The rate at which latent tuberculosis develops into active tuberculosis in people living with HIV
γ	Treatment rate per capita for people with active tuberculosis
γ_0	Rate of treatment for latent tuberculosis patients
γ_1	Treatment rate for co-infected people with latent tuberculosis and HIV
γ_2	Rate of treatment for co-infected active tuberculosis
E_1	Rate of bacterial shedding by persons with active tuberculosiss $[A_T]$.
E_2	Co-infected individuals' bacterial shedding rate $[M_2]$.
M	Rate of environmental bacterial clearance.

Proof. Standard results for Caputo fractional differential equations with spatially Lipschitz right-hand sides imply existence and uniqueness [11]. By calculating each state variable's Caputo derivative on the non-negative orthant's border, positivity is confirmed. For instance, we have ${}_0^cD_t^\omega S(t) = \rho^\omega > 0$, if $S = 0$, then the trajectories stay non-negative. For any compartment, the same argument holds

□

Theorem 3.2. *Every system (2.5) solution that starts in the physiologically feasible area*

$$\Gamma = \begin{cases} S, L_T, A_T, R_T, E_b, H_I, A_H, M_1, M_2, C_T \in R_+^{10} \\ P \leq \frac{\rho^\omega}{N_d^\omega}, E_b \leq \frac{(E_1^\omega + E_2^\omega)\rho^\omega}{E^\omega N_d^\omega} \end{cases} . \tag{3.1}$$

Remain in Γ *for all* $t > 0$.

Proof. The linear fractional differential equation for $P(t)$ that results from adding the human population equations is bounded above by $\frac{\rho^{\omega}}{N_d^{\omega}}$. The model's mathematical soundness and epidemiological importance are confirmed by these results, which also apply to the environmental bacterial load E_b. □

3.1. Disease-Free Equilibrium and Reproduction Threshold Analysis. Setting all infected compartments to zero yields the system's HIV-TB co-infection free equilibrium (DFE).

$$E_0 = (S^0, L_T^0, A_T^0, R_T^0, E_b^0, H_I^0, A_H^0, M_1^0, M_2^0, C_T^0) = \left(\frac{\rho^{\omega}}{N_d^{\omega}}, 0, 0, 0, 0, 0, 0, 0, 0, 0\right) \tag{3.2}$$

We use the next generation matrix approach, which was developed in [12], to calculate the fundamental reproduction number R_0 in order to examine the risk of disease transmission. The average number of secondary infections that an infected person causes in a community that is fully susceptible during their infectious period is indicated by the basic reproduction number. The disease's independence at the DFE determines the total basic reproduction

$$R_0 = max(R_0^{TB}, R_0^{HIV}) \tag{3.3}$$

Where

$$R_0^{TB} = \frac{\Lambda_1^{\omega}(\rho^{\omega}\alpha_1^{\omega}E_1^{\omega} + \alpha_T^{\omega}E^{\omega}N_d^{\omega})}{N_d^{\omega}(N_d^{\omega} + \Lambda_1^{\omega} + \gamma_0^{\omega})E^{\omega}(d_T^{\omega} + N_d^{\omega} + \gamma^{\omega})} \tag{3.4}$$

and

$$R_0^{HIV} = \frac{\alpha_H^{\omega}}{N_d^{\omega} + d_H^{\omega} + \xi^{\omega}} \tag{3.5}$$

The amount R_0^{TB} highlights the relevance of bacterial persistence in maintaining TB spread by capturing both environment-mediated and direct TB transmission. The balance between HIV transmission and treatment-induced elimination is represented by the HIV reproduction number R_0^{HIV}. Appendix B has the complete derivation, which includes Jacobian matrices.

3.2. Evaluation of the Disease-Free State's Local Stability. We investigate the local asymptotic stability of the disease-free equilibrium (DFE) E_0, a state that is free of both HIV and TB. An eigen value-based approach modified from [13] is used to investigate small perturbations at E_0. The following theorem establishes the stability requirement

Theorem 3.3. *When $R_0 < 1$ and unstable $R_0 > 1$, the disease-free equilibrium E_0 of the system is locally asymptotically stable.*

Proof. The outcome is obtained by looking at the eigenvalues of the Jacobian matrix evaluated at E_0 and using the fractional order stability criterion, which calls for all eigen values to satisfy $|arg(\lambda_i)| > \frac{\pi\omega}{2}$. According to this analysis, both HIV and TB can be eradicated from an epidemiological perspective if their respective reproduction numbers are lowered below unity.

3.3. Existence and Ulam-Hyers Stability Analysis. The practical usefulness of a model is contingent upon its ability to withstand perturbations, such as those resulting from numerical approximation or parameter uncertainty. We analyze our fractional order system's Ulam-Hyers stability, which ensures that approximation solutions stay near to genuine solutions under minor shocks, in order to prove this characteristic.

Theorem 3.4. *The Caputo fractional-order HIV-TB co-infection model exhibits Ulam-Hyers stability on the time interval* $[0, P]$ *if the following is true:*

$$\Gamma(\omega + 1) = KP^{\omega}.$$

Where K is the model vector field's Lipschitz constant.

Proof. Ulam-Hyers stability guarantees that approximate solutions remain near precise solutions even in the presence of small perturbations to the governing equations. For models that have been calibrated using real epidemiological data, this feature is particularly important. Classical Lyapunov stability, on the other hand, examines the behavior of exact solutions under slightly different initial conditions.

3.4. Numerical Solution of the Caputo Fractional-Order System Using the PECE-ABM Method. The Predict-Evaluate-Correct-Evaluate Adams-Bashforth-Moulton (PECE-ABM) algorithm, a multi-step method chosen for its effectiveness in addressing the memory integrals inherent in fractional derivatives, was used to create numerical solutions for the Caputo of fractional-order systems [14]. The PECC-ABM approach uses an implicit corrector step (Adams-Moulton) after an explicit predictor step (Adams-Bashforth). We discretize the temporal domain into grid points $T_k = kH$ and define a fixed step size H for numerical implementation. Weights are used in the anticipated phase to take the beginning value problem into account.

$$C_{l,k+1} = \frac{H^T}{T}[k + 1 - l]^T - (k - l)^T$$

To produce the anticipated values

$$\overline{y_{n+1}} = y_0 + \frac{1}{\Gamma(p)} \sum_{i=0}^{k} C_{l,k+1} G_l$$

Which are then evaluated to obtain
$\overline{G_{k+1}} = G(T_{k+1}, \overline{y_{k+1}})$ The corrector stage then uses weights to improve the answer.

$$D_{l,k+1} = \frac{h^T}{T(T+1)}[k + 1 - l]^{T+1} - (k - l)^{T+1}$$

Producing
$R_{k+1} = R(T_{k+1}, Y_{k+1})$ is the new evaluation of the modified solution. All model compartments, including susceptible, infected, and treated populations, are subjected to this iterative prediction-evaluation-correction-evaluation method. The population size and the force of infection are updated at every stage. The method can be used to simulate both controlled and uncontrolled models. since it guarantees accurate and steady numerical integration of the fractional order dynamics.

3.5. Estimation of Model Parameters World. Health Organisation reported HIV-TB co-infection data for Tanzania from 2000 - 2023, given as cases per 1,000,000 people, were used to estimate system parameters. The aggregated, anonymised, and publicly accessible data does not require ethical approval. Active TB co-infection compartment $M_2(t)$, The model was calibrated by fitting a model that reflects the synergistic HIV-TB interaction driving transmission and environmental contamination and accurately fits the provided data. The model structure implicitly constrained all other compartments. To ensure biological survival, initial circumstances were created using 2000 demographic and epidemiological data. M_2 (0)=309 infected compartments were inferred from prevalence statistics, treated compartments were first thought to be negligible, and the ambient TB load was computed proportionately to infectious TB cases. By minimizing the difference between the model-predicted co-infected population and the observed HIV-TB co-infection data, parameters were determined.

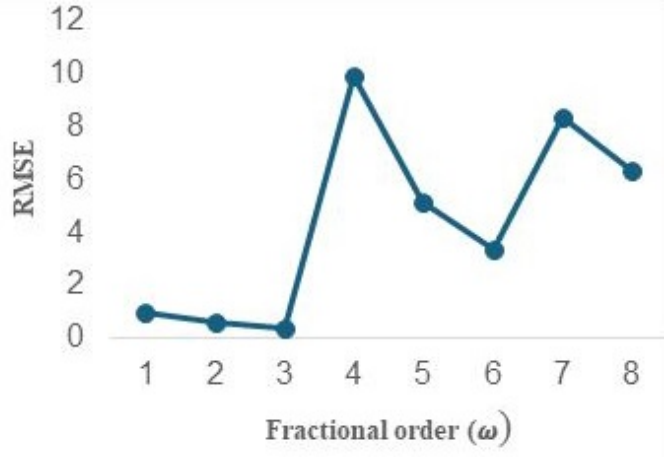
Let $M_2^{model}(t_i/\theta)$ represent the corresponding model output for a parameter vector θ, and $M_2^{data}(t_i)$ represent the reported HIV-TB co-infection data at time t_i. The root mean square error (RMSE) was used to define the goal function as

$$RMSE(\theta) = \left[\frac{1}{n}\sum_{n=1}^{n}(M_2^{data}(t_i)) - (M_2^{model}(t_i|\theta))^2\right]^{\frac{1}{2}} \tag{3.6}$$

where θ and n = 24 represent specific environmental, transmission, and progression characteristics. The PECE-ABM scheme described in was used to solve the fractional system, and the novel Nelder-Mead simplex algorithm [16] in MATLAB was used for optimization. National life expectancy statistics were used to determine demographic factors. With an average life expectancy of roughly 66.8 years [15], Tanzania has a national mortality rate of $N_d = 1/66.8 \approx 0.0147 year^{-1}$, with recruitment adjusted to preserve demographic balance. The fit quality was assessed using the root mean square error (RMSE), which reached a minimum value of 8.06 at the fractional order $\omega = 0.982$. The best fractional derivative order for the given data is $\omega = 0.982$, as seen by the RMSE decreasing as ω approaches 0.982 and increasing for lower values. displays the model estimations for this ideal order. The fractional order model ($RMSE = 8.06,\ R^2 = 0.9915$) performs better than the integer order model ($RMSE = 8.39,\ R^2 = 0.9907$), delivering a roughly 4% reduction in RMSE and a slightly enhanced goodness of fit, according to a comparison of the predictions from the two models.

3.5.1. *Empirical Validation of the Model.* Kenya was chosen because it is geographically close to Tanzania [17] and has similar epidemiological and socioeconomic characteristics, even though it represents a separate population. Assuming that fundamental biological and behavioral processes are conserved throughout East African environments, all epidemiological parameters obtained from Tanzanian data were kept. Based on a life expectancy of 66.8 years, the recruitment rate (ρ=7.8 persons per 1,00,000 annually) and natural mortality rate (N_d=0.0150 annually) were the only demographic parameters that were modified to reflect Kenya-specific characteristics. HIV-TB prevalence in 2000 [18]. Through 2023, the model (ω=0.982) was simulated and compared to actual data. RMSE, MAPE, and R^2 were used to assess the model's performance on the validation dataset. The results showed good prediction accuracy: RMSE = 13.17, MAPE = 21.18 %, and $R^2 = 0.9601$. The model accurately captured important temporal aspects of Kenya's HIV-TB co-infection dynamics, such as the maximum between 2005-2007 and

FIGURE 2. Analysis of Root Mean Square Error (RMSE) across derivative orders



the subsequent decline following ART scale-up. The resilience of the fractional-order framework is demonstrated by the deviation seen at the peak period, which most likely reflects variations in intervention coverage or behavioral characteristics not reflected by demographic parameter adjustments.

3.6. Global Sensitivity Analysis. A sensitivity analysis of the fundamental reproduction numbers R_0 is carried out in order to assess the relative impact of model parameters. This kind of study determines which parameters have the biggest effects on the dynamics of disease transmission and measures how minor adjustments to these parameters alter the model's results. The impact of a minor percentage change in a parameter K on the reproduction number is computed using the normalized forward sensitivity index [19]. The sensitivity of R_0^{TB} or R_0^{HIV} to its parameters is evaluated using the index $\gamma_K = \frac{K}{R_0^{TB}} \frac{R_0^{TB}}{\partial K}$ Model parameter sensitivity indices for the fundamental reproduction numbers R_0^{TB} and R_0^{HIV}

TABLE 2

Parameter	Index	Parameter	Index	Parameter	Index
ρ	0.8924	d_T	0.475	α_T	0.3105
E_1	0.8924	d_H	0.4682	∂	0
Λ_1	0.5	α_H	1	E	-0.6023
N_d	0.1603	α_1	0.8902	ξ	-0.4605
γ	-0.4738	γ_0	-0.7817		

Table 2 displays the resulting indices, calculated at at $\omega = 0.982$. The calculated sensitivity indices reveal an important finding: whereas positively sensitive factors like E_1, α_T, α_H and α_1 encourage disease spread, raising the negatively sensitive parameters (γ, ξ, E) substantially

decreases disease dynamics, hence offsetting transmission. Quantitatively, for every 10% rise in E and ξ, R_0^{TB}or R_0^{HIV} are decreased by 7.9% and 5.7%, respectively. The selection of the multifaceted environmental and medicinal controls described in section 4 is directly informed by and validated by this mechanistic understanding. To evaluate the resilience of these sensitivity values under parameter uncertainty, confidence intervals for the normalized sensitivity indices were computed using a Monte Carlo uncertainty propagation technique. The fractional order model's analytical equations were used to recalculate sensitivity indices for every realization, and model parameters were sampled from truncated normal distributions that matched the predicted means and 95% confidence intervals given in Table 4. The percentile distributions of the resulting sensitivity indices, from which empirical 95% confidence intervals were obtained, are summarized in Table 3. Critical transmission and treatment parameters show confidence intervals that do not include zero, and the results confirm that the sign and relative ranking of the most critical parameters remain unchanged throughout uncertainty ranges, supporting the robustness of the sensitivity conclusions.

4. Controlled Dynamical System

$$
\begin{aligned}
{}_0^cD_t^\omega S(t) &= \rho^\omega - (F_T^c + F_H^c + N_d^\omega)S \\
{}_0^cD_t^\omega L_T(t) &= F_T^c S + \partial F_T^c R_T - (N_d^\omega + \Lambda_1^\omega + \gamma_0^\omega + \Theta_1 + F_H^c)L_T \\
{}_0^cD_t^\omega A_T(t) &= \Lambda_1^\omega L_T - (N_d^\omega + d_T^\omega + \gamma^\omega + \Theta_1 + F_H^c)A_T \\
{}_0^cD_t^\omega R_T(t) &= (\gamma^\omega + \Theta_1)A_T + (\gamma_0^\omega + \Theta_1)L_T - (N_d^\omega + \partial F_T^c + F_H^c)R_T \\
{}_0^cD_t^\omega E_b(t) &= E_1^\omega A_T + E_2^\omega M_2 - (E^\omega + \Theta_3)E_b \\
{}_0^cD_t^\omega H_I(t) &= F_H^c S + F_H^c R_T - (N_d^\omega + d_H^\omega + \Delta F_T^c + \xi^\omega + \Theta_2)H_I \\
{}_0^cD_t^\omega A_H(t) &= (H_I + C_T)(\xi^\omega + \Theta_2) - (N_d^\omega + d_H^\omega)A_H \\
{}_0^cD_t^\omega M_1(t) &= F_H^c L_T - (N_d^\omega + \Lambda_2^\omega + d_H^\omega + \gamma_1^\omega + \Theta_1)M_1 \\
{}_0^cD_t^\omega M_2(t) &= \Lambda_2^\omega M_1 + \Delta F_T^c H_I + F_H^c A_T - (N_d^\omega + d_e^\omega + \gamma_2^\omega + \Theta_1)M_2 \\
{}_0^cD_t^\omega C_T(t) &= (\gamma_1^\omega + \Theta_1)M_1 + (\gamma_2^\omega + \Theta_1)M_2 - (N_d^\omega + \xi^\omega + \Theta_2 + d_e^\omega)C_T \\
With\ \ F_T^C &= [\frac{\alpha_T^\omega}{P}(A_T + \mu_1 M_2) + \alpha_1^\omega E_b]\ \ and\ \ F_H^C = \frac{\alpha_H^\omega}{P}(H_I + \mu_2 M_1)
\end{aligned}
\tag{4.1}
$$

4.1. Evaluation of the Effective Reproduction Number R_e. The dynamics of HIV-TB co-infection and the effects of intervention strategies are evaluated using the effective reproduction number R_e for the system is calculated as follows using the next generation matrix approach [21] and the methodology described in section 3.2. This amount measures the expected number of new infected originating from a single infectious individual in a largely managed population [20].

$$R_e = max(R_e^{TB}, R_e^{HIV}) \tag{4.2}$$

FIGURE 3. Model Fits and HIV-TB co-infection prevalence in Tanzania from 2000 to 2023

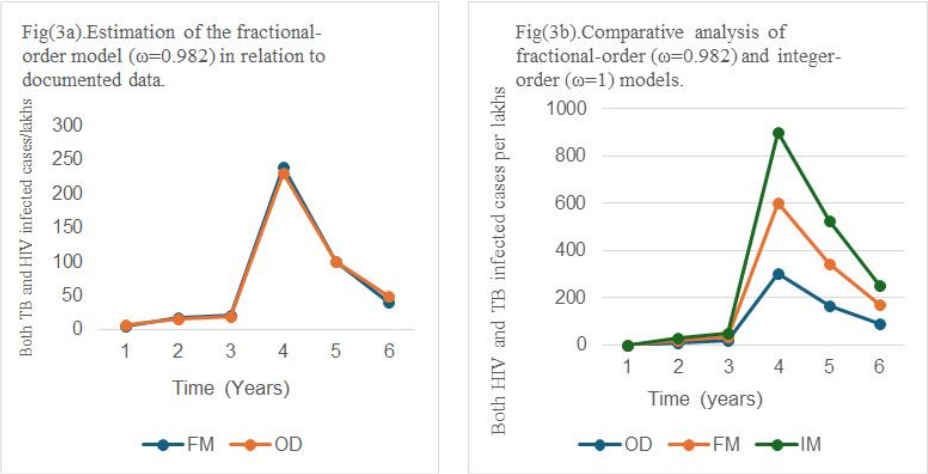


TABLE 3

R_0^{TB}			R_0^{HIV}		
Parameter	**Mean**	95%	**Parameter**	**Mean**	95%
ρ	0.8924	[0.7661,0.7981]	N_d	-0.1544	[0.5928,0.-5592]
E_1	0.8424	[0.7661,0.7981]	ξ	-0.6872	[-0.5928, -0.5592]
Λ_1	0.8403	[0.7468,0.7695]	α_H	0.9931	[0.9820,0.9820]
N_d	-0.8203	[-0.9503, -0.9174]	d_H	-0.4737	[-0.3791,-0.3460]
γ	-0.5429	[-0.4494,-0.4144]			
d_T	-0.5993	[-0.5070,-0.4709]			
α_1	0.8835	[0.7661,0.7981]			
γ_0	-0.7776	[-0.6802,-0.6543]			
E	-0.8935	[-0.7981,-0.7661]			

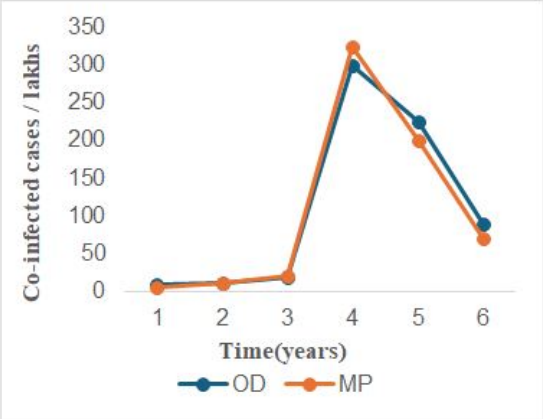
The two illnesses' effective reproduction numbers are calculated independently since they are independent at the DFE. The TB subsystem's effective reproduction number is

$$R_e^{TB} = \frac{\Lambda_1^\omega(\rho^\omega \alpha_1^\omega E_1^\omega + \alpha_T^\omega E^\omega N_d^\omega + \alpha_T^\omega N_d^\omega \Theta_3)}{N_d^\omega(N_d^\omega + \Lambda_1^\omega + \gamma_0^\omega + \Theta_1)(E^\omega + \Theta_3)(d_T^\omega + N_d^\omega + \gamma^\omega + \Theta_1)} \tag{4.3}$$

and $R_e^{HIV} = \frac{\alpha_H^\alpha}{N_d^\omega + d_H^\omega + \xi^\omega + \Theta_2}$ These expressions account for transmission from individuals with active tuberculosis, the contaminated environment, and direct HIV transmission-all of which are impacted by the restrictions put in place. The findings highlight the theoretical impact

of the interventions: improving TB case detection and treatment TB $[\Theta_1(t)], ART[\Theta_2(t)]$ and environmental cleanliness and sanitation $[\Theta_3(t)]$ directly lowers the co-infection's potential for transmission.

FIGURE 4. Validation of the fractional-order HIV-TB co-infection model using Kenyan data (2000-2023). Place your order at ($\omega = 0.982$)



4.2. Optimal Control Analysis. The polluted environment E_B, which acts as a transmission reservoir, and the infected classes $(L_T, A_T, H_I, M_1, M_2)$, which are the main dispersion drivers, are the two main compartments that support HIV-TB co-infection. In order to create the best control methods, we concentrate on minimizing these compartments. Therefore, minimizing the sizes of L_T, A_T, H_I, M_1, M_2, and E_B targets both direct transmission channels and important behavioral variables, creating a goal that is both epidemiologically sound and pertinent to policy. Therefore, based on the system, we want to find an ideal control triple $\Theta_1, \Theta_2, \Theta_3$ that lowers the cost of control measures, environmental contamination, and sick populations. In accordance with the objective fractional related framework, which is defined as:

$$\begin{aligned} I(\Theta_1, \Theta_2, \Theta_3) &= \int_0^P \left[A_1 L_T + A_2 A_T + A_3 H_I + A_4 M_1 + A_5 M_2 + A_6 E_b + \tfrac{1}{2} \textstyle\sum_{i=1}^{3} (\acute{N}_i \Theta_i^2) dt \right] \\ &= \int_0^P \sigma(t, x, u) dt \end{aligned} \tag{4.4}$$

$\sigma(t, x, u)$ represents the running cost. For a given co-state variable λ_n, the associated Hamiltonian is given by the associated Hamiltonian is given by

$$H = \sigma(t, x, u) + \Sigma_{n=1}^{10} \lambda_n f_n(t, x, u) \tag{4.5}$$

The relative importance of the state variables is quantified by the positive constants $A_i (i = 1, 2, 3, 4, 5, 6)$, and the costs of applying the control measures across the finite time horizon P are represented by $\acute{N}_i, (i = 1, 2, 3)$ [22,23]. These constants keep the integral in the objective functional from being dominated by any one term. Furthermore, in the case of

computation, the objective function is stated quadratically [24, 25]. For i=1,2,3, the admissible control set is determined by $\Theta = (\Theta_1, \Theta_2, \Theta_3)/\Theta_i$ is Lebesgue measurable and $0 \leq \Theta \leq 1, t \in [0, P]$ The optimal control $\Theta^* = (\Theta_1^*, \Theta_2^*, \Theta_3^*)$ minimizes the objective functional: $J(\Theta^*) = \underset{(\Theta_1, \Theta_2, \Theta_3) \in U}{min} J(\Theta_1, \Theta_2, \Theta_3)$ Classical results ensure that an optimal control exists under the well-posed nature of the state system and the uniform L_∞ restrictions on admissible states and controls [26,27]. Pontryagin's Maximum principle, The necessary optimality conditions for the control Θ^*.are found using a modified version for fractional order systems controlled by the Caputo derivative. This concept transforms the objective functional equation and the system equation into a pointwise minimization of the Hamiltonian (H) with regard to the controls $(\Theta^*(t))$. For the fractional adjoint system, the fractional state dynamics, and the associated stationary conditions to continue being optimal. Adjoint system and stationary conditions are obtained from the related fractional state dynamics as follows: The state dynamics given by ${}_0^C D_t^\omega f_n = \frac{\partial H}{\partial \lambda_n}$, and adjoint system given by ${}_0^C D_t^\omega \lambda_n = -\frac{\partial H}{\partial x_n}$. Therefore, the system of adjoint variable takes the form:

$$
\begin{aligned}
{}_0^C D_t^\omega \lambda_S(t) &= F_T^C(\lambda_S - \lambda_{L_T}) + F_H^C(\lambda_S - \lambda_{H_I}) + N_d^\omega \lambda_S \\
{}_0^C D_t^\omega \lambda_{L_T}(t) &= -A_1 + F_H^C(\lambda_{L_T} - \lambda_{M_1}) + \Lambda_1^\omega(\lambda_{L_T} - \lambda_{A_T}) \\
&\quad +(\gamma_0^\omega + \Theta_1)(\lambda_{L_T} - \lambda_{R_T}) + N_d^\omega \lambda_{L_T} \\
{}_0^C D_t^\omega \lambda_{A_T}(t) &= -A_2 + \partial \frac{\alpha_T^\omega}{P} R_T(\lambda_{R_T} - \lambda_{L_T}) + \frac{\alpha_T^\omega}{P} S(\lambda_S - \lambda_{L_T}) \\
&\quad +\Delta \frac{\alpha_T^\omega}{P} H_I(\lambda_{H_I} - \lambda_{M_2}) + (\gamma^\omega + \Theta_1(t))(\lambda_{A_T} - \lambda_{R_T}) \\
&\quad -E_1^\omega \lambda_{E_B} + (N_d^\omega + d_T^\omega)\lambda_{A_T} - F_H^C \lambda_{A_T} \\
{}_0^C D_t^\omega \lambda_{R_T}(t) &= \partial F_T^C(\lambda_{R_T} - \lambda_{L_T}) + F_H^C(\lambda_{R_T} - \lambda_{H_I}) + N_d^\omega \lambda_{R_T} \\
{}_0^C D_t^\omega \lambda_{E_B}(t) &= -A_6 + \alpha_1^\omega \Delta(\lambda_S - \lambda_{L_T}) + \partial \alpha_1^\omega(\lambda_{R_T} - \lambda_{L_T}) R_T + \\
&\quad \alpha_1^\omega \Delta I_T(\lambda_{I_T} - \lambda_{M_2}) + (E^\omega + \Theta_3(t))\lambda_{E_B} \\
{}_0^C D_t^\omega \lambda_{H_I}(t) &= -A_3 + \frac{\alpha_H^\omega}{P} S(\lambda_S - \lambda_{H_I}) + \frac{\alpha_H^\omega}{P} R_T(\lambda_{R_T} - \lambda_{H_I}) \\
&\quad +\frac{\alpha_H^\omega}{P} L_T(\lambda_{L_T} - \lambda_{M_1}) + \frac{\alpha_H^\omega}{P} A_T(\lambda_{A_T} - \lambda_{M_2}) \\
&\quad +(\xi^\omega + \Theta_2(t))(\lambda_{H_I} - \lambda_{A_H}) + \Delta F_T^C(\lambda_{H_I} - \lambda_{M_2}) + (N_d^\omega + d_H^\omega)\lambda_{H_I} \\
{}_0^C D_t^\omega \lambda_{A_H}(t) &= (N_d^\omega + d_H^\omega)\lambda_{A_H} \\
{}_0^C D_t^\omega \lambda_{M_1}(t) &= -A_4 + \mu_2 \frac{\alpha_H^\omega}{P} S(\lambda_S - \lambda_{H_I}) + \mu_2 \frac{\alpha_H^\omega}{P} R_T(\lambda_{R_T} - \lambda_{H_I}) \\
&\quad +\mu_2 \frac{\alpha_H^\omega}{P} A_T(\lambda_{A_T} - \lambda_{M_2}) + \mu_2 \frac{\alpha_H^\omega}{P} L_T(\lambda_{L_T} - \lambda_{M_1}) \\
&\quad (\gamma_1^\omega + \Theta_1(t))(\lambda_{M_1} - \lambda_{C_T}) + \Lambda_2^\omega(\lambda_{M_1} - \lambda_{M_2}) + (N_d^\omega + d_H^\omega)\lambda_{M_1}
\end{aligned}
$$

$$
\begin{aligned}
{}_0^C D_t^{\omega}\lambda_{M_2}(t) &= -A_5 + \mu_1\frac{\alpha_T^{\omega}}{P}S(\lambda_S - \lambda_{L_T}) + \mu_1\partial\frac{\alpha_T^{\omega}}{P}R_T(\lambda_{R_T} - \lambda_{L_T}) \\
+\mu_1\Delta\frac{\alpha_T^{\omega}}{P}H_I(\lambda_{H_I} - \lambda_{M_2}) &+ (\gamma_2^{\omega} + \Theta_1(t))(\lambda_{M_2} - \lambda_{C_T}) - E_2^{\omega}\lambda_{E_b} + (N_d^{\omega} + d_e^{\omega})\lambda_{M_2} \\
{}_0^C D_t^{\omega}\lambda_{C_T}(t) &= (\xi^{\omega} + \Theta_2(t))(\lambda_{C_T} - \lambda_{A_H}) + (N_d^{\omega} + d_e^{\omega})\lambda_{C_T}
\end{aligned} \tag{4.6}
$$

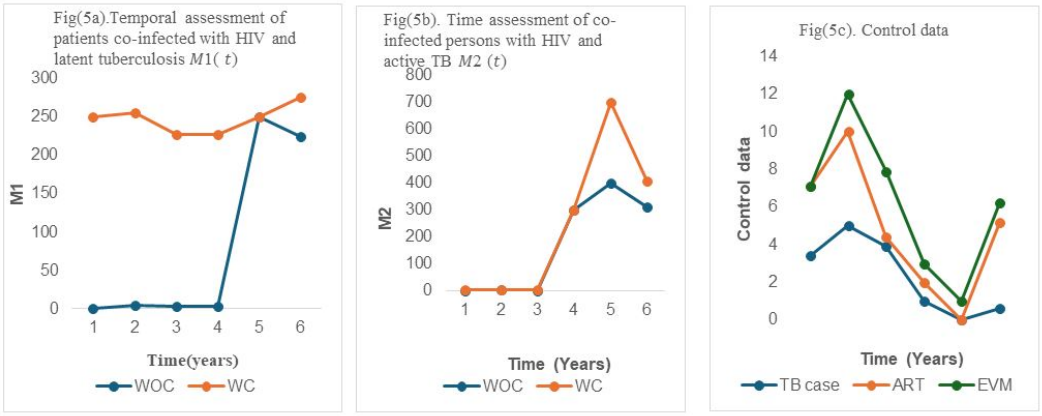
The terminal condition $\lambda_n(P) = 0$ is satisfied by every adjoint variable $\lambda_n(t)$. For $n = S, L_T, A_T, R_T, E_b, H_I, A_H, M_1, M_2, C_T(1-10)$ the stationary conditions are derived by solving $\frac{\partial H}{\partial \Theta_i} = 0$, i various from 1 to 3

$$
\begin{aligned}
\Theta_1^* &= \frac{1}{N_1}\begin{bmatrix} L_T^*(\lambda_{L_T} - \lambda_{R_T}) + A_T^*(\lambda_{A_T} - \lambda_{R_T}) \\ +M_1^*(\lambda_{M_1} - \lambda_{C_T}) + M_2^*(\lambda_{M_2} - \lambda_{C_T}) \end{bmatrix} \\
\Theta_2^* &= \frac{1}{N_2}[H_I^*(\lambda_{H_I} - \lambda_{A_H}) + C_T^*(\lambda_{C_T} - \lambda_{A_H})] \\
\Theta_3^* &= \frac{1}{N_3}[E_b^*\lambda_{E_b}]
\end{aligned} \tag{4.7}
$$

The optimal controls Θ_i^* i various from 1 to 3 are restricted to the interval [0,1] and enforced through the projection formula

$$\Theta_i^* = max\{0, min(\Theta_i, 1)\}$$

FIGURE 5. Impact of strategy A, which combines HIV and TB treatment, at ($\omega = 0.982$)



5. Numerical Investigation and Discussion

The Caputo-type fractional order system is numerically solved using the PECE-ABM scheme described to determine the optimal control strategies Θ^* for reducing the transmission of HIV-TB co-infection. The forward-backward sweep method updates the control variables until convergence while iteratively integrating the state system ahead and the adjoint system backward

FIGURE 6. Impact of combining environmental sanitation and hygiene with TB treatment (strategy B) at (ω=0.982)

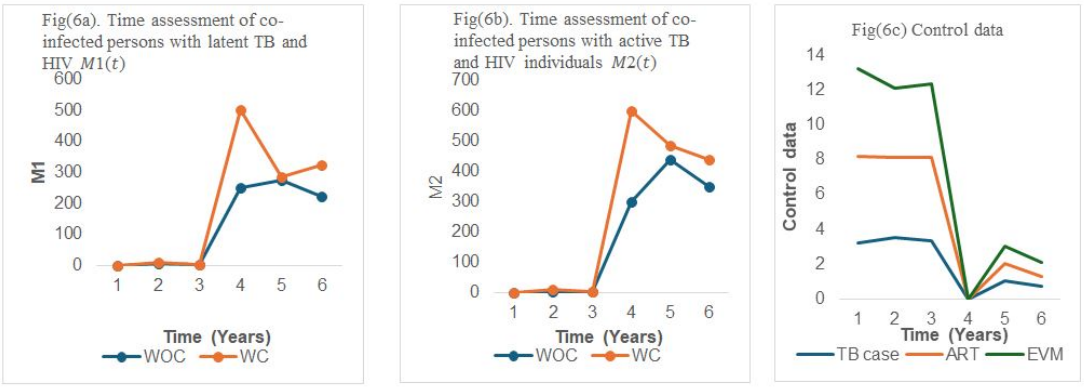
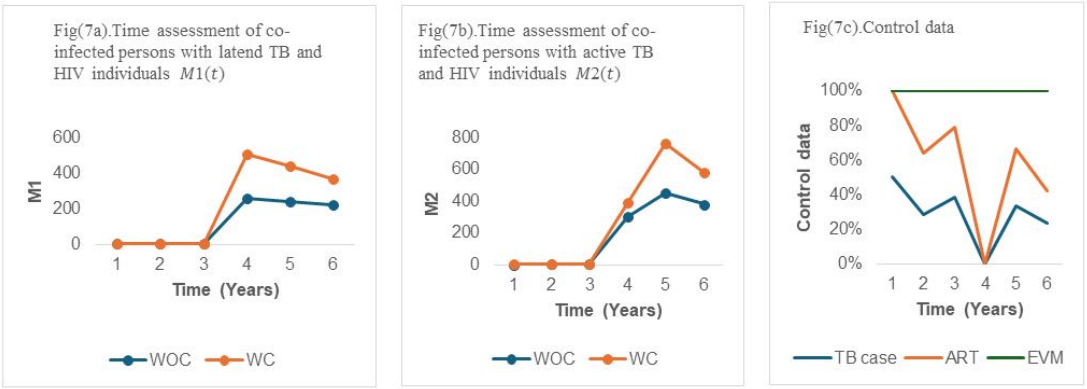
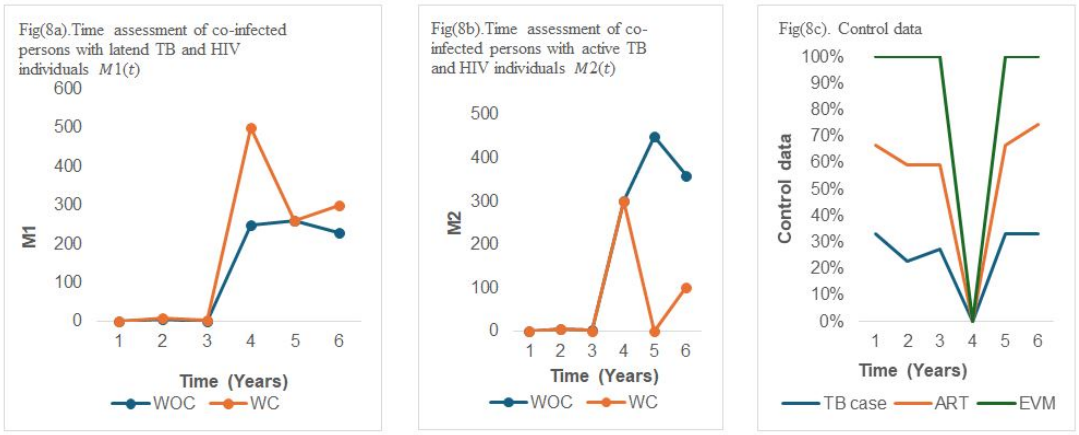


FIGURE 7. Impact of combining environmental sanitation and hygiene with HIV treatment (strategy C) at (ω=0.982)



[28]. This approach guarantees numerical correctness and stability while successfully capturing the memory effects present in fractional-order dynamics. The cost weights w_i in the objective functional in optimal control issues indicate the relative financial burden of carrying out each intervention. In order to prevent unrealistic singular control solutions, these weights are provided to balance epidemiological advantages against implementation costs. They are often modeled using quadratic terms to penalize excessive control effort and assure conductivity of the goal functional [29,35]. The approximate annualized per-capita cost reported in health economic research from Tanzania and comparable sub-Saharan African contexts was represented by the weights w_1, w_2, and w_3 in this study. In this case, w_1, w_2, and w_3 stand for environmental control, HIV therapy, and TB treatment interventions, respectively, as mentioned in section 4.

FIGURE 8. Impact of combining environmental sanitation and hygiene with HIV treatment and TB treatment (strategy D) at ($\omega = 0.982$)



The estimated annual cost of diagnosing and treating a single case of tuberculosis in Tanzania is between 150 - 155 per person. Consequently, USD/person/year, a conservative estimate within this range, was determined as the weight for the TB treatment control. The projected annual cost of ART for HIV treatment in Tanzania is between USD 90 and USD 265 per person. This range was used to generate a mid-range estimate for the weight associated with HIV treatment, which was set at $w_2 = 150$ USD/person/year. Disinfection, better ventilation, and sanitation are examples of environmental treatments that are usually carried out at the community level and involve common, non-recurring costs as opposed to individualized therapeutic expenditures [30,31,40]. The cost weight for environmental control was set at around 36% of the cost of TB treatment in order to account for this difference, resulting in $w_3 = 54$ UST/person/year. This assumption maintains the relative cost structure of controls while reflecting the relatively lower per-capita economic impact of environmental actions. In general, These weights are meant to offer a realistic and policy-relevant scale of intervention costs so that the best management options can be meaningfully compared, rather than to represent exact economic figures. The waiting parameters of the objective functional represent the severity of each compartment. Since it is less contagious than people in other affected compartments, the weight G_i linked with compartment L is given a weight in the limit [0, 0.5]. Because of their comparatively smaller immediate health and economic effects in comparison to co-infected compartments. The interval [0.5,1.5] is used to select the weights G_2 and G_3 corresponding to compartments A_T and H_I.To represent their enhanced severity, the co-infected compartments M_1 and M_2 are given higher weights, $G_4 \in [1, 5]$ and $G_5 \in [5, 10]$, respectively. $G_6 \in [0, 0.5]$ penalizes the ambient bacterial load E_b, which leads to protracted infection and disease recurrence [32,33,41]. As shown in Table 4, initial circumstances are set appropriately, and model parameters are established using actual data and existing literature. Due to data scarcity, which continues to be a significant limitation in modelling HIV-TB co-infection dynamics, some parameters are chosen only for numerical illustration [36,37]. The uncertainty in parameter estimations resulting from

the absence of high resolution, longitudinal data on ambient TB contamination, co-infection rates, and behavioral variables is demonstrated by the huge confidence ranges for several fitted parameters. This uncertainty spreads throughout the model, impacting both the projected timing of intervention effects and the accuracy of long-term forecasts [34,35,38]. For example, changes in the bacterial clearance rate E and environmental transmission rate α_1 could affect the expected timing and size of the effects of environmental interventions. From a policy standpoint, this means that rather than using exact quantitative projections, model outputs should be interpreted mainly in a comparative and strategic sense, guiding the relative efficacy and prioritization of integrated initiatives [39,40]. Model predictions and policy recommendations can be improved as more specific data becomes available. To run the simulations and validate the analytical results, MATLAB is used. For both controlled and uncontrolled scenarios, state trajectories and control profiles are examined. We assess the efficacy of many concurrent control measures over a five-year period, taking into account the endemicity of HIV-TB co-infection as well as the limited impact of single therapies [42,43].

6. Conclusion

To better represent disease dynamics, this group created a Caputo type fractional-order model of HIV-TB co-infection that took memory effects and environmental TB reservoirs into account by confirming the existence, uniqueness, positivity, boundedness, and Ulam-Hyers stability of solutions, it was demonstrated that the model was mathematically well-posed. The prerequisites for disease elimination were verified by local stability analysis and the derivation of basic reproduction numbers. An ideal fractional order of ω=0.982 was obtained by parameter estimation using Tanzania data (2000-2023), which provided excellent agreement with reported observations. The model's resilience and transferability were confirmed by validation using Kenyan data. The fractional formulation better captured long-term disease persistence and delayed treatment effects as compared to the traditional integer-order model. Treatment rates, transmission coefficients, and environmental clearance were found to be important factors influencing transmission dynamics through sensitivity analysis. The integrated approach that combined TB therapy, ART, and environmental sanitation proved to be the most successful in lowering co-infection prevalence and attaining disease eradication, according to optimal control outcomes. These results highlight the significance of coordinated environmental and therapeutic strategies for HIV-TB management, especially in high-burden settings. To further improve the model's suitability for public health decision-making, future research should include behavioral aspects, stochastic impacts, regional heterogeneity, and cost-effectiveness analysis.

References

1. Adesola, O.I., Temilade, M.I., Emmanuel, P.M., Oladele, A.S., Adeyemi, A.G., Sunday, S., Olumuyiwa, A.S., 2024. Mathematical analysis of optimal control of human immunodeficiency virus (HIV) co-infection with tuberculosis (TB). *Asian Res. J. Curr. Sci. 23-53.*
2. Adeyemo, S., Sangotola, A., Korosteleva, O., 2023. Modeling transmission dynamics of tuberculosis-HIV co-infection in South Africa. *Epidemiologia 4 (4), 408-419*
3. Singh, R., Ali, S., Jain, M., et al., 2016. Epidemic model of HIV/AIDS transmission dynamics with different latent stages based on treatment. *Am. J. Appl. Math 4, 222-234.*

4. Devi, A.S., Naik, P.A., Boulaaras, S., Sene, N., Huang, Z., 2025. Understanding the transmission mechanism of HIV/TB co-infection using fractional framework with optimal control. *Int. J. Numer. Modelling, Electron. Netw. Devices Fields 38 (4), e70097.*
5. Khan, M.A., Ullah, S., Kumar, S., 2021. A robust study on 2019-nCOV outbreaks through non-singular derivative. *Eur. Phys. J. Plus 136 (2), 168.*
6. Ayele, T.K., Doungmo Goufo, E.F., Mugisha, S., 2024a. Co-infection mathematical model for HIV/AIDS and tuberculosis with optimal control in Ethiopia. PLOS ONE 19 (12), e0312539. *http://dx.doi.org/10.1371/journal.pone.0312539*
7. Gao, C., Zhang, T., Liao, Y., Wang, Y., Jiao, H., Wu, M., Cui, Q., Wang, K., Wang, L., 2024. Modelling of tuberculosis dynamics incorporating indirect transmission of contaminated environment and infectivity of smear-negative individuals: A case study for Xinjiang, China. *Acta Trop. 254, 107130. http://dx.doi.org/10.1016/j. actatropica.2024.107130.*
8. Angstmann, C.N., Henry, B.I., McGann, A.V., 2016. A fractional-order infectivity SIR model. *Phys. A 452, 86-93.*
9. Pinto, C.M., Carvalho, A.R., 2017. A latency fractional order model for HIV dynamics. *J. Comput. Appl. Math. 312, 240-256.*
10. Ruoja, C.S., Nyerere, N., Mayengo, M.M., Nyabadza, F., 2025. Dynamic and optimal control of TB transmission: the role of vaccination funding and social processes using Caputo-type framework. *Int. J. Dyn. Control. 13 (12), 414.*
11. Bolaji, B., Onoja, T., Benedict, A.C., Omede, B.I., Odionyenma, U.B., 2024. Dynamical analysis of HIV-TB co-infection transmission model in the presence of treatment for TB. *Bull. Biomath. 2 (1), 21-56. http://dx.doi.org/10.59292/bulletinbiomath. 2024002*
12. Naik, P.A., Yavuz, M., Qureshi, S., Zu, J., Townley, S., 2020a. Modeling and analysis of COVID-19 epidemics with treatment in fractional derivatives using real data from Pakistan. *Eur. Phys. J. Plus 135, 1-42. http://dx.doi.org/10.1140/epjp/s13360-020- 00840-9*
13. Edward, S., 2024. A fractional order model for the transmission dynamics of shigellosis. *Heliyon 10 (10).*
14. Naik, P.A., Zu, J., Owolabi, K.M., 2020b. Global dynamics of a fractional order model for the transmission of HIV epidemic with optimal control. *Chaos Solitons Fractals 138, 109826.*
15. World Health Organization, 2023b. Life expectancy, united Republic of tanzania, 2023. *https://data.who.int/countries/834.* (Accessed 10 April 2025).
16. Chinyoka, M., Gashirai, T.B., Mushayabasa, S., 2021. On the dynamics of a fractional- order Ebola epidemic model with nonlinear incidence rates. *Discrete Dyn. Nat. Soc. 2021 (1), 2125061. http://dx.doi.org/10.1155/2021/2125061.*
17. World Health Organization, 2023a. Global tuberculosis programme data,2023. *https: //www.who.int/teams/global-tuberculosis-programme/data.* (Accessed 10 April 2025).
18. World Health Organization, 2023c. Life expectancy, Republic of Kenya, 2023. *https: //data.who.int/countries/404.*(Accessed 3 February 2026).
19. Chitnis, N., Hyman, J.M., Cushing, J.M., 2008. Determining important parameters in the spread of malaria through the sensitivity analysis of a mathematical model. *Bull. Math. Biol. 70, 1272-1296. http://dx.doi.org/10.1007/s11538-008-9299-0.*
20. Stephano, M.A., Mayengo, M.M., Irunde, J.I., 2024. The role of asymptomatic carriers on the dynamics of a lymphatic filariasis model incorporating control strategies. *Results Control. Optim. 15, 100425.*
21. Naik, P.A., Yavuz, M., Qureshi, S., Zu, J., Townley, S., 2020a. Modeling and analysis of COVID-19 epidemics with treatment in fractional derivatives using real data from Pakistan. *Eur. Phys. J. Plus 135, 1-42. http://dx.doi.org/10.1140/epjp/s13360-020- 00840-9*
22. Ullah, A., Sakidin, H., Gul, S., Alharthi, T.N., Metwally, D.S., Hamed, Y., Shah, K., Sambas, A., 2025. Exploring the effectiveness of an optimal control model for Marijuana consumption. *Eur. J. Pure Appl. Math. 18 (3), 6451-6451.*
23. Kheiri, H., Jafari, M., 2018. Optimal control of a fractional-order model for the HIV/AIDS epidemic. *Int. J. Biomath. 11 (07), 1850086. http://dx.doi.org/10.1142/ S1793524518500869.*
24. Karim, M., Kouidere, A., Rachik, M., Shah, K., Abdeljawad, T., 2023. Inverse problem to elaborate and control the spread of COVID-19: A case study from Morocco. *AIMS Math. 8 (10), 23500-23518.*

25. Li, Q., Wang, F., 2023. An epidemiological model for tuberculosis considering environmental transmission and reinfection. *Mathematics 11 (11), 2423.*
26. Pontryagin, L.S., 2018. Mathematical Theory of Optimal Processes. Routledge.
27. Lenhart, S., Workman, J.T., 2007. Optimal Control Applied to Biological Models. *Chapman and Hall /CRC.*
28. McAsey, M., Mou, L., Han, W., 2012. Convergence of the forward-backward sweep method in optimal control. *Comput. Optim. Appl. 53, 207-226. http://dx.doi.org/ 10.1007/s10589-011-9454-7.*
29. Sadek, L., Ounamane, S., Abouzaid, B., & Sadek, E. M. (2024). The Galerkin Bell method to solve the fractional optimal control problems with inequality constraints. *Journal of Computational Science, 77, 102244.*
30. Sadek, L., & Akgül, A. (2024). New properties for conformable fractional derivative and applications. Progr. Fract. Differ. Appl, 10(3), 335-344.
31. Sadek, L., & Talibi Alaoui, H. (2023). Numerical methods for solving large-scale systems of differential equations. *Ricerche di Matematica, 72(2), 785-802.*
32. Sadek, L., & Alaoui, H. T. (2022). Application of MGA and EGA algorithms on large-scale linear systems of ordinary differential equations. *Journal of Computational Science, 62, 101719.*
33. Sadek, L., & Talibi Alaoui, H. (2020). The extended block Arnoldi method for solving generalized differential Sylvester equations. *Journal of Mathematical Modeling, 8(2), 189-206.*
34. Sadek, L., & Algefary, A. (2025). On quantum trigonometric fractional calculus. *Alexandria Engineering Journal, 120, 371-377.*
35. Sadek, L. (2025). Control theory for fractional differential Sylvester matrix equations with Caputo fractional derivative. *Journal of Vibration and Control, 31(9-10), 1586-1602.*
36. Sadek, L., & Alaoui, H. T. (2021). The extended nonsymmetric block lanczos methods for solving large-scale differential lyapunov equations. *Math. Model. Comput, 8(3), 526-536.*
37. Alqhtani. M., Sadek, L., & Saad, K. M. (2025). The Mittag-Leffler-Caputo-Fabrizio fractional derivative and its numerical approach. *Symmetry, 17(5), 800.*
38. Harshita Kaushik, Vijai Shanker Verma, Ram Singh. A. Manickam Assesing the effects of vaccination on Tuberculosis and COVID-19 co-infection modelling. *Contemporary Mathematics volume 6 issue 1 PP-222-245 ISSN: 2705-1064. (ESCI, Scopus) [2025].*
39. A. Manickam, M. Kavitha, A. Benevatho Jaison, Arvind Kumar Singh A fractional-order mathematical model of Banana Xanthomonas Wilt disease using Caputo derivatives. *Contemporary Mathematics ISSN: 2705-1064. (ESCI, Scopus). [2024]*
40. Pushpendra Kumar · Vedat Suat Erturk · Swati Tyagi · Jozef Banas ·A. Manickam .,A generalized Caputo-type fractional-order neuron model under the electromagnetic field. *International Journal of Dynamics and Control, Electronic ISSN 2195-2698 Print ISSN 2195-268X (ESCI-Scopus) https://doi.org/10.1007/s40435-023-01134-4. [2023]*
41. Pushendra Kumar Norodin A. Rangaig, Hamadjam Abboubakar Anoop Kumar & A. Manickam Prediction studies of the epidemic peak of coronavirus disease in Japan: From Caputo derivatives to Atangana-Baleanu derivatives. *International Journal of Modeling, Simulation, and Scientific Computing 2250012 (32 pages) (Scopus Indexed & Web of Science, Impact factor 1.2). [2022]*
42. M. Sharmila and S. Indrakala Fractional-Order Modeling and Neural Network Simulation of NKCell- Oncolytic Virus Interactions. *International Journal of Basic and Applied Sciences, volume 14, issue:8 106-120 https://doi.org/10.14419/9pjcye33(2025)*
43. M. Sharmila and S. Indrakala Novel Approaches to Positive Solutions for Fractional Nonlinear Boundary Value Problems Page no 2254-2265 Volume 6 Issue 2—2025— ISSN: 2705-1064 (Print) 2705-1056 (Online).

G. Karuppannan: School of Sciences, Division of Mathematics, SRM Institute of Science and Technology, Tiruchirappalli Campus, Tiruchirappalli -621105. Tamilnadu, India.
Email address: karuppannanlakphd@gmail.com

A. Manickam: School of Sciences, Division of Mathematics, SRM Institute of Science and Technology, Tiruchirappalli Campus, Tiruchirappalli -621105. Tamilnadu, India.
Email address: manickammaths2011@gmail.com